CFAR STAP Radar using Compressive Sensing for Random Arrays

Haley H. Kim
UNITED STATES OF AMERICA

Hkim82488@gmail.com

Alexander M. Haimovich
UNITED STATES OF AMERICA

haimovic@njit.edu

ABSTRACT

In this paper, we present CFAR detectors for STAP random arrays. The problem is formulated as detection of sparse targets given space-time observations from thinned random arrays. The observations are corrupted by colored Gaussian noise of unknown covariance matrix, but secondary data is available for estimating the covariance matrix. New CFAR detectors are developed that cope with the high sidelobes of random arrays. Analysis demonstrate high performance with significantly fewer elements than a ULA.

1.0 INTRODUCTION

Ground moving target indicator (GMTI) radar is an airborne radar mounted on an aircraft that detects the presence of targets on the ground. One of the main challenges faced by GMTI radars is the detection of slow moving targets in the presence of ground clutter interference. Space-time adaptive processing (STAP) implemented with antenna arrays has been a classical approach to clutter cancellation in airborne radar [1]. One of the challenges with STAP is that the minimum detectable velocity (MDV) of targets is a function of the baseline of the antenna array: the larger the baseline (i.e. the narrower the beam), the lower the MDV. Unfortunately, increasing the baseline of a uniform linear array (ULA) entails a commensurate increase in the number of elements.

An alternative approach to increasing the resolution of a radar, but without using a large number of sensors is to use a large, but sparsely populated array. In a sparse array, the sensors are placed across a large array with interelement spacing greater than half a wavelength in a nonuniform manner to avoid grating lobes. Since the resolution of the radar depends mostly on the size of the aperture [2], a radar utilizing a sparse array may achieve a high angular resolution with significantly fewer sensors than a ULA. One simple method to populate the large array with nonuniform sensor positions, is to place the sensors across a large array aperture randomly, which is referred to as random arrays [2],[3]. Unfortunately, sparse arrays do not come without drawbacks. Due to the spatial undersampling, the array beampattern suffers from high sidelobes. During the beamforming stages of STAP, these high sidelobes may cause a significant increase in false alarms [4].

In [5], Carin demonstrates that measurements from random arrays are consistent to projection measurements that can be utilized by compressive sensing (CS) [6]. This suggests that the user may reap the full benefits of a large random array without worrying that the high sidelobes unnecessarily increase the false alarm rate. The goal of CS is to recover the signal of interest $\mathbf{x}$, given the received data vector $\mathbf{y}$ and a linear model $\mathbf{y}=\mathbf{A}\mathbf{x}+\mathbf{e}$, where $\mathbf{A}$ is a measurement matrix and $\mathbf{e}$ is an interference vector. If the signal $\mathbf{x}$ is known to be sparse (i.e. contains K

nonzero elements where K is much smaller than the number of entries in **x**), the K sparse solution (a solution with at most K nonzero entries) may be found solving the nonconvex optimization problem

$$\min_{\mathbf{x}} \ \|\mathbf{y}-\mathbf{A}\mathbf{x}\|_0 \ \text{ subject to } \ \|\mathbf{x}\|_0 \le K \tag{1}$$

where $\|\mathbf{x}\|_0$ counts the numbers of non-zero elements in $\mathbf{x}$. The above optimization problem is nonconvex, and only approximate solutions can be obtained. A popular approach to solving (1) is to use Matching Pursuit (MP) algorithms [7]-[11]. MP belong to the class of greedy algorithms, which search iteratively one-by-one for components of the unknown vector **x**. Components of **x** detected by MP iterations are removed from subsequent iterations to reduce interference to components of **x** yet to be detected. MP algorithms are a popular and attractive choice because of their lower computational complexity [12]. A large body of literature exists on CS applications to radar, but the literature on applying MP to CFAR radar is scarce, with some exceptions, e.g. [10], [13]. In particular [13], does not account for colored Gaussian noise and unknown interference covariance matrix.

In this paper, we extend the work in [13] and propose new detection algorithms for airborne radar, which combine the strengths of random arrays with the ability of sparsity based algorithms to handle undersampling effects. We propose a sparsity-based CFAR detection algorithms, referred to as MP-CFAR. MP-CFAR consists of a target localization stage followed by a target detection stage.

2.0 SIGNAL MODEL

In this section, we introduce the STAP radar signal model and discusses properties of random arrays in STAP radar. Consider a radar system mounted on an aircraft, in which N_a elements collect returns of a narrowband transmitted signal consisting of an N_p-pulse coherent waveform with pulse-repetition-interval T_r. The radar operating carrier wavelength is λ, and the airborne platform velocity is v_p, where the velocity vector is assumed aligned with the array axis. The N_a receive sensor locations $z_1, z_2, \ldots z_{N_a}$ are assumed to be chosen randomly within an aperture of length *Z*, where the sensor locations and the aperture length are expressed in units of the wavelength λ. For concreteness, it is assumed that the positions of receive elements are drawn from a uniform distribution. An example of an array is shown in Figure 1.

Let $u = \sin\theta$ denote the spatial frequency associated with the azimuth angle measured with respect to the normal to the array. The $N_a \times 1$ array response vector $\mathbf{c}(u)$, is defined

$$\mathbf{c}(u) = \frac{1}{\sqrt{N_a}}\left[e^{j2\pi z_1 u}, e^{j2\pi z_2 u}, \ldots, e^{j2\pi z_{N_a} u}\right]^T. \tag{2}$$

Since by applying the vector $\mathbf{c}^*(u)$ the array is steered to spatial frequency u, $\mathbf{c}(u)$ is also known as a *steering vector*.

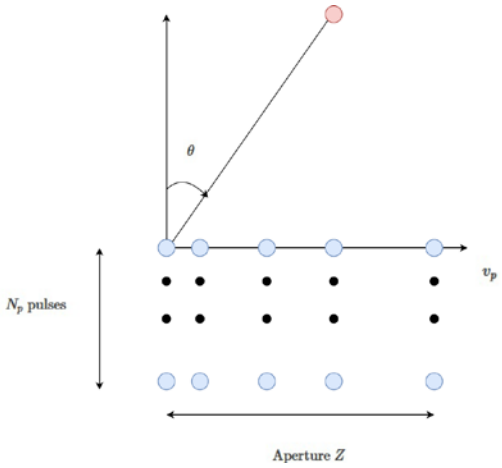

Figure 1: STAP random array radar system model

The Doppler shift caused by a target moving at velocity v_t relative to the normal to the array is $f_d = 2v_t / \lambda$. The normalized Doppler frequency v is the Doppler shift f_d normalized to the sampling frequency $1/T_r$, where T_r is the pulse repetition interval, $v = f_d T_r$. The $N_p \times 1$ temporal steering vector $\mathbf{g}(v)$ of a target with normalized Doppler frequency v is given by

$$\mathbf{g}(v) = \frac{1}{\sqrt{N_p}}\left[1, e^{j2\pi v}, , \ldots, e^{j2\pi(N_p-1)v}\right]^T. \tag{3}$$

For notational convenience, let $N = N_a N_p$, then the $N \times 1$ space-time steering vector of a target with spatial frequency u and Doppler v is given by

$$\mathbf{a}(u,v) = \mathbf{g}(v) \otimes \mathbf{c}(u) \tag{4}$$

where, $\otimes$ represents the Kroneckor product. The $N \times 1$ baseband $\mathbf{y}$ signal received at the array from a target with steering vector $\mathbf{a}$ and complex amplitude x is given by

$$\mathbf{y} = \mathbf{a}x + \mathbf{e} \tag{5}$$

where $\mathbf{e} = \mathbf{e}_c + \mathbf{e}_w$ is the interference vector consisting of the ground clutter contributions $\mathbf{e}_c$ and complex-valued white Gaussian noise $\mathbf{e}_w$. We treat ground clutter and thermal noise as uncorrelated processes, and therefore the $N \times N$ interference and noise covariance matrix is given by

$$\mathbf{R} = \mathrm{E}\left[(\mathbf{e}_c + \mathbf{e}_w)(\mathbf{e}_c + \mathbf{e}_w)^H\right] = \mathbf{R}_c + \mathbf{R}_w. \tag{6}$$

Here $\mathbf{R}_w$ is the covariance matrix of the thermal noise given by $\mathbf{R}_w = \sigma^2\mathbf{I}$ where σ^2 is the power of thermal noise. A typical model for the clutter covariance matrix $\mathbf{R}_c$ [14] is

$$\mathbf{R}_c = \int_{-1}^{1} s(u)\mathbf{a}\left(u,\xi u\right)\mathbf{a}^H\left(u,\xi u\right)du \tag{7}$$

The signal model for K targets is given by

$$\mathbf{y} = \mathbf{A}\mathbf{x} + \mathbf{e}, \tag{8}$$

where, $\mathbf{A}$ is the $N \times G$ measurement matrix whose columns are steering vectors associated with a grid of possible target locations on the angle-Doppler map and $\mathbf{x}$ is a $G \times 1$ vector of complex target amplitudes. The vector $\mathbf{x}$ contains only $K \ll G$ nonzeros. In later sections, we apply optimization algorithms that operate on a grid. To this end, we discretize the angle-Doppler map into $G = \bar{G}^2$ grid points, where $\bar{G}$ is the number of grid points in each of the two domains. The G grid points serve as resolution cells. Typically the dimensionality of the signal space N is much smaller than the number of resolution cells, $N \ll G$. Therefore, the $G \times 1$ vector of target gains $\mathbf{x}$ is assumed to be sparse, in the sense that it has $K \ll G$ nonzero entries.

In STAP, the covariance matrix $\mathbf{R}$ is typically unknown, but can be estimated from *secondary data*. The secondary data is assumed to consist of independent identically distributed vectors with a covariance matrix common with the cell under test. Let L be the number of secondary data vectors and $\mathbf{q}(l)$ a secondary data vector, the maximum likelihood estimate (MLE) of the covariance matrix is the sample covariance matrix

$$\hat{\mathbf{R}} = \frac{1}{L}\sum_{l=1}^{L}\mathbf{q}(l)\mathbf{q}(l)^H. \tag{9}$$

In subsequent sections, we will make use of the inverse of the sample covariance matrix. In order to ensure that $\hat{\mathbf{R}}^{-1}$ exists, we make the assumption that $L > N$.

In random arrays, antenna elements are placed at random between the end points of an array. Since the goal is to obtain a thinned array, the average spacing between antenna elements is larger than half-wavelength. Thus, the term "random arrays" refers to arrays that are thinned relative to a filled ULA.

STAP relies on the fact that the rank of the clutter covariance matrix $\mathbf{R}_c$ (often referred to as *clutter rank*) is rank deficient. As a result, whitening of the clutter interference does not result in significant loss of target SNR. In a filled ULA, the clutter map (defined as $\mathbf{a}^H(u,v)\mathbf{R}_c\mathbf{a}(u,v)$, with u and v sweeping through their domains $|u| < 1,\ |v| < 1$), forms a diagonal ridge above the *uv* plane. The width of the ridge along the spatial frequency u axis equals the beamwidth of the array. Thus the clutter ridge of a random array is expected to be narrower than the clutter ridge of a filled ULA with the same number of elements. This is illustrated in Figure 2.

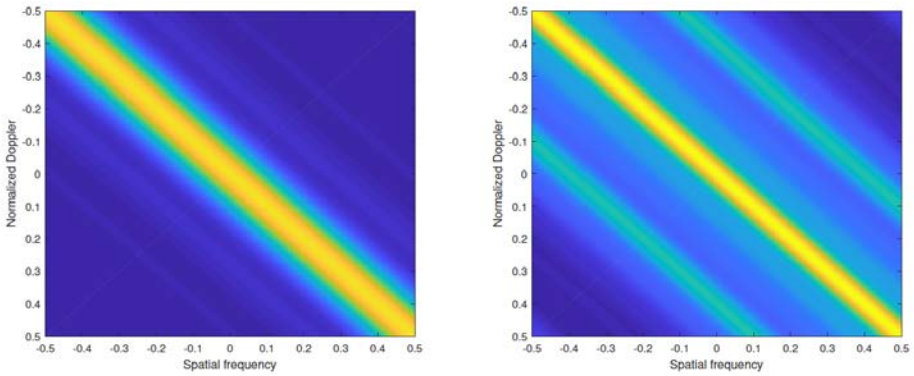

Figure 2:(Left figure): Clutter map using a ULA with $N=10$ elements, $P=20$ pulses, and $\xi=1$. (Right figure): Clutter map using a random array with $N=10$ elements, $P=20$ pulses, and $\xi=1$. The elements of the sparse random array are spread across an array of size 15λ.

The panel on the left of Figure 2 shows the clutter map of a ULA with $N=10$ elements, while the panel on the right shows the clutter map of a random array of the same number of elements (10) spread over 15λ (rather than the 5λ ULA aperture), both the clutter maps are generated with $\xi=1$. It is noticed that the clutter ridge of the random array is narrower, which leads to a lower MDV. Note that the clutter map of the sparse array also exhibits multiple, spurious clutter ridges due to higher sidelobes of the beampattern.

The clutter rank of a filled ULA can be computed from Brennan's rule

$$r_c = \text{rank}(\mathbf{R}_c) = N_a + (N_p - 1)\xi, \tag{10}$$

where recall that $\xi = 2v_p T_r / \lambda$. Now, given a random array with aperture size Z, let N_a^{full} represent the number of sensors in a filled ULA configuration. From [15] the clutter rank of a random array is

$$\overline{r_c} \approx N_a^{full} + (N_p - 1)\xi. \tag{11}$$

It is noticed that the clutter rank of a random array depends on the aperture size Z, since $N_a^{full} = 2Z$. This means the random array will require the same number of degrees of freedom to suppress the clutter as a large ULA. However, the number of degrees of freedom available to the random array is less than that of the large ULA. Therefore, fewer degrees of freedom are left to supply gain for the target than for the filled ULA.

3.0 STAP DETECTION PROBLEM

In this section, we introduce the detection problem in addition, we present the CS optimization problem in order to introduce the sparsity based detection problem. Detection by AMF [16] is agnostic to the possible presence of multiple targets, the AMF does not take into account any potential interference caused by targets. When a ULA is employed, the sidelobes are considered negligible and hence, it is often not necessary to consider the potential

interference between targets. However, a random array exhibits large sidelobes and hence this assumption is no longer true. In contrast, the model (8) accounts for multiple targets. As explained previously, the number of rows of $\mathbf{A}$, N, is much smaller than the number of columns G. The problem of recovering $\mathbf{x}$ given $\mathbf{y}$ and $\mathbf{A}$ is then underdetermined, and hence does not have a unique solution. Instead, inspired by compressive sensing techniques, we seek to solve the following optimization problem

$$\min_{\mathbf{x}} \|\mathbf{y}-\mathbf{A}\mathbf{x}\|_0 \text{ subject to } \|\mathbf{x}\|_0 \le K \tag{12}$$

where $\|\mathbf{x}\|_0$ denotes the number of nonzero elements of $\mathbf{x}$. As previously discussed, problems involving the zero norm are non-convex, and their solution implemented by an exhaustive search among all combinations of non-zero indices of $\mathbf{x}$, requires exponential complexity [17]. Matching pursuit (MP) is a practical complexity algorithm whose solution approximates the solution to (12). However, MP is not directly applicable to the radar problem for two reasons; (1) it does not take into account the presence of clutter, and (2) in radar, the number of targets K is not known apriori. Proposed solutions to address these problems as well as various enhancements are the presented in this section.

In radar, clutter contributions are typically much stronger than the unknown targets and, if not suppressed, may severely interfere with target detection. A whitening operation is applied to the observed data and to the measurement matrix $\mathbf{A}$. Specifically, let $\mathbf{z}=\hat{\mathbf{R}}^{-1/2}\mathbf{y}$ and $\mathbf{B}=\hat{\mathbf{R}}^{-1/2}\mathbf{A}$, then (13) becomes

$$\min_{\mathbf{x}} \|\mathbf{z}-\mathbf{B}\mathbf{x}\|_0 \text{ subject to } \|\mathbf{x}\|_0 \le K \tag{13}$$

Unfortunately, to solve (14) one requires the knowledge of number of targets K, which of course is unknown apriori. In the next section we propose a sparsity based algorithm that circumvents the need to have apriori knowledge of the number of targets K.

4.0 MP-CFAR

To implement a CFAR radar that exploits target sparsity, we propose the two-stage MP-CFAR detection algorithm. Candidate targets are localized in the first phase; in the second phase, the candidate targets are tested for detection. A detected target is then cancelled from the data. The cancellation of detected targets from the data is intended to remove mutual interference between targets. A block diagram of the MP-CFAR algorithm is shown in Figure 3.

4.1 Stage 1: MP Localization

The first pass of the MP localization algorithm uses whitened data $\mathbf{z}=\hat{\mathbf{R}}^{-1/2}\mathbf{y}$ and whitened steering vectors $\mathbf{b}_j=\hat{\mathbf{R}}^{-1/2}\mathbf{a}_j$, $j=1,...,G$. The first candidate target is localized by the index m_1 of the vector $\mathbf{b}_j$ that has the largest data projection,

$$m_1 = \arg\max_j \frac{|\mathbf{b}_j^H \mathbf{z}|^2}{\mathbf{b}_j^H \mathbf{b}_j} \tag{14}$$

for $j = 1, \ldots, G$. The index m_1 localizes the target in the angle-Doppler domains. This information is subsequently used by the detection stage, as described in relation with Stage 2 below.

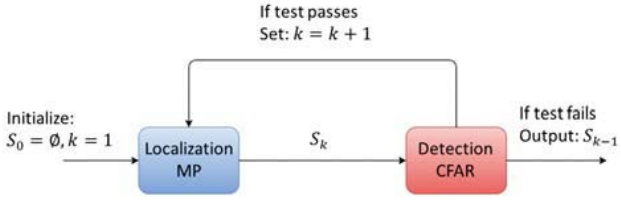

Figure 3: Block diagram of the MP-CFAR algorithm.

Next, we describe the localization of the k-th candidate target, given that $k-1$ targets have already been localized and passed the detection test. The observed and whitened data $\mathbf{z}$ is processed to cancel the contribution of targets detected previously. Let a matrix $\mathbf{B}$ be formed with the columns $\mathbf{b}_j$. Let S_{k-1} be the set of indices of columns of $\mathbf{B}$ associated with detected targets, and let $\mathbf{B}_{S_{k-1}}$ be the matrix formed by the columns indexed by S_{k-1}. The projection matrix orthogonal to the detected targets is given by $\mathbf{P}^{\perp}_{\mathbf{B}_{S_{k-1}}} = \mathbf{I} - \mathbf{B}_{S_{k-1}} \left(\mathbf{B}^H_{S_{k-1}} \mathbf{B}_{S_{k-1}} \right)^{-1} \mathbf{B}_{S_{k-1}}$. Similarly, steering vectors orthogonal to the detected targets are formed as follows: $\mathbf{w}_j = \mathbf{P}^{\perp}_{\mathbf{B}_{S_{k-1}}} \mathbf{b}_j$, for all $j \notin S_{k-1}$. The k-th target is localized according to

$$m_k = \arg\max_j \frac{|\mathbf{w}_j^H \mathbf{z}|^2}{\mathbf{w}_j^H \mathbf{w}_j}. \tag{15}$$

This process continues until a candidate target fails the detection test.

4. 2 Stage 2: Detection

We now describe the CFAR detector that is applied to candidate targets localized in Stage 1. The first candidate target is detected according to the AMF test statistic [16]

$$T = \frac{|\mathbf{a}_{m_1}^H \hat{\mathbf{R}}^{-1} \mathbf{y}|^2}{\mathbf{a}_{m_1}^H \hat{\mathbf{R}}^{-1} \mathbf{a}_{m_1}} \geq \gamma \ , \tag{16}$$

where m_1 is the index found in Stage 1. Note that the test (16) may also be expressed in terms of the whitened steering vectors $\mathbf{b}_{m_1} = \hat{\mathbf{R}}^{-1/2} \mathbf{a}_{m_1}$,

$$T = \frac{|\mathbf{b}_{m_1}^H \mathbf{z}|^2}{\mathbf{b}_{m_1}^H \mathbf{b}_{m_1}} \geq \gamma \ . \tag{17}$$

Next we describe the detection of candidate target k, given that $k-1$ targets have been already localized and passed the detection test. The signal model is given by the expression

$$\mathbf{z} = \mathbf{b}_{m_k} x_{m_k} + \mathbf{B}_{S_{k-1}} \mathbf{x}_{S_{k-1}} + \mathbf{n} \ = \mathbf{B}_{S_k} \mathbf{x}_{S_k} + \mathbf{n} \tag{18}$$

where m_k is the index of the resolution cell of the k-th candidate target found in Stage 1 (15), S_k is formed by adding m_k to the set S_{k-1}, $S_k = S_{k-1} \bigcup m_k$, the matrix $\mathbf{B}_{S_k} = \left[\mathbf{b}_{m_k}, \mathbf{B}_{S_{k-1}} \right]$ is the matrix formed by columns with indices in S_k, $\mathbf{x}_{S_k} = \left[x_{m_k}, \mathbf{x}_{S_{k-1}}^T \right]^T$, and $\mathbf{n} = \hat{\mathbf{R}}^{-1/2} \mathbf{e}$. This signal model leads to the following detection test:

$$H_0 : x_{m_k} = 0 ; \ \ H_1 : x_{m_k} \neq 0 .$$

Here, the following problem is posed: detect a target located at a specified whitened steering vector $\mathbf{b}_{m_k}$ and having unknown amplitude, observed in the presence of interference and noise. The interference is of unknown gain $\mathbf{x}_{S_{k-1}}$, but belonging to a known subspace $\mathbf{B}_{S_{k-1}}$. The noise is Gaussian colored noise for which the covariance matrix is unknown, but secondary data is available for its estimation.

To develop the test statistic for the detection problem, we start by expressing the likelihoods of the observations under the two hypotheses. As in the discussion in [16], the detector is a generalized likelihood ratio detector only in the sense that the likelihood under H_1 is maximized over the unknown target amplitude. To simplify the detector, as in [16], it is assumed that the pdf's of the test statistic under each hypothesis are based on the true covariance matrix. It is noted that the subsequent analysis relies on the properties of the estimated covariance matrix. Thus, $\mathbf{z} = \hat{\mathbf{R}}^{-1/2} \mathbf{y}$ is modeled as having a covariance matrix equal to the identity matrix. It follows that under H_0, the likelihood is

$$p\left(\mathbf{z} \,|\, \mathbf{H}_0\right) = \frac{1}{\pi^N} e^{-\left(\mathbf{z}-\mathbf{B}_{S_{k-1}}\mathbf{x}_{S_{k-1}}\right)^H \left(\mathbf{z}-\mathbf{B}_{S_{k-1}}\mathbf{x}_{S_{k-1}}\right)} ,$$

while under H_1 the likelihood is

$$p\left(\mathbf{z} \,|\, \mathbf{H}_1\right) = \frac{1}{\pi^N} e^{-\left(\mathbf{z}-\mathbf{B}_{S_k}\mathbf{x}_{S_k}\right)^H \left(\mathbf{z}-\mathbf{B}_{S_k}\mathbf{x}_{S_k}\right)} .$$

The GLRT for deciding H_1 is given by

$$T = \ln\left(\frac{\max_{\mathbf{x}_{S_k}} p(\mathbf{z}\,|\,\mathbf{x}_{S_k})}{\max_{\mathbf{x}_{S_{k-1}}} p(\mathbf{z}\,|\,\mathbf{x}_{S_{k-1}})}\right) \geq \gamma\,. \tag{19}$$

It can be shown that the test statistic (19) can be simplified to

$$T = \|\mathbf{z} - \mathbf{B}_{S_k}\mathbf{x}_{S_k}\|_2^2 - \|\mathbf{z} - \mathbf{B}_{S_{k-1}}\mathbf{x}_{S_{k-1}}\|_2^2 = \mathbf{z}^H\left(\mathbf{P}_{\mathbf{B}_{S_k}} - \mathbf{P}_{\mathbf{B}_{S_{k-1}}}\right)\mathbf{z} \tag{20}$$

Therefore, in order to test the k-th candidate target, we first generate the subspace $\mathbf{B}_{S_k}$, we then generate the interference subspace, $\mathbf{B}_{S_{k-1}} = \mathbf{B}_{S_k}$, k and apply (20). The test statistic (20) is applied to every candidate target included in the set S_k. If any of the k tests fails to exceed the threshold γ, the algorithm terminates and outputs the set S_{k-1}, the set of $k-1$ target locations. Otherwise, MP-CFAR increments the number of targets k by one and reruns MP with the new value of k.

5.0 NUMERICAL SIMULATIONS

In this section, we present numerical results on the MP-CFAR algorithm and compare them with AMF. Unless stated otherwise, in figures presented in this section, the aperture of the random arrays is 12λ ($Z = 12$, where Z is expressed in units of wavelength). The number of elements in the random array is $N_a = 16$, thus the mean spacing between elements of the random array is $12\lambda/16$. The number of coherent pulses used by all arrays is $N_p = 25$. The SNR, defined as $|x|^2/\sigma^2$ is set to SNR = 15.5 dB unless stated otherwise. The clutter-to-noise ratio (CNR) is set to 30 dB. It was seen that the SINR of the random array defined as $\text{SINR}_i = \mathbf{a}_i^H\mathbf{R}^{-1}\mathbf{a}_i$ is roughly 15 dB with these parameters. The number of training samples used to estimate the covariance matrix for the random array is $L = 2N$. The number of resolution cells on the angle-Doppler map is given by $G = (2Z+1)^2 = 625$. A random realization of a random array is generated and remains fixed throughout the Monte Carlo simulations for all figures unless otherwise stated. Let S_t be the true set of resolution cells that contain targets, and let $\hat{S}$ be the set of resolution cells found by a detector to have targets. A false alarm event occurs is $\hat{S}$, $S_t \neq \varnothing$, and a detection event occurs if $\hat{S}\bigcap S_t \neq \varnothing$. Unless specified, the threshold parameter was chosen such the probability of false alarm is 10^{-3}. The equation

$$\gamma_{ABF} = \frac{L+1}{L-N+1}\left[(P_{FA})^{\frac{1}{L-N+2}}\right]$$

found in [18] was used to find the appropriate value of γ_{AMF} for the AMF. It can be shown that corresponding threshold parameter for MP-CFAR is given by

$$\gamma_{MP} = \frac{L+1}{L-N+1}\left[(P_{FA}^{MP})^{\frac{1}{L-N+2}} \right]$$

where $P_{FA}^{MP} = 1-(1-P_{FA})^{1/G}$. The value P_{FA}^{MP} is used instead of P_{FA} because the MP-CFAR and algorithm utilize the maximization operation.

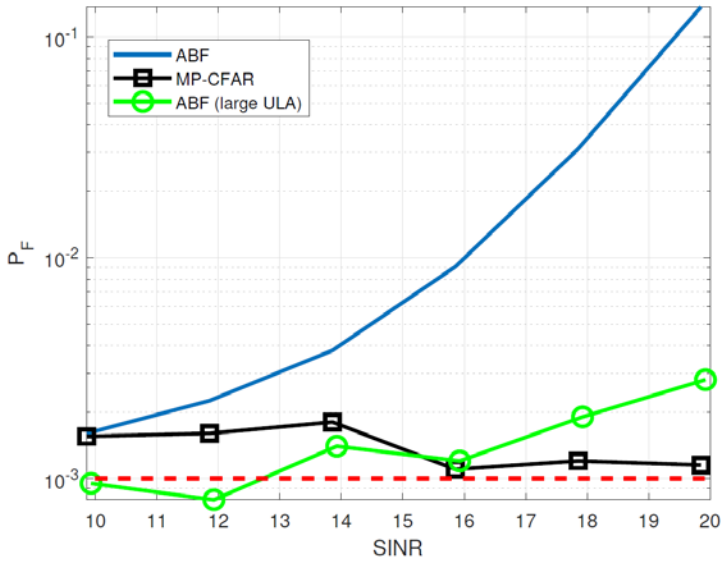

Figure 4: Probability of false alarm vs SINR of a target for the AMF with a random array, MP-CFAR with a random array, and the AMF with a large ULA.

The probabilities of false alarm of the MP-CFAR and AMF detectors are studied in Figure 4, which plots the empirical probability of false alarm against the SINR of a target present with the angle-Doppler pair (5/Z,0). In this figure, the arrays compared are a 12λ ULA and an 12λ random array. The random array has $N_a = 16$ sensors, the resolution cells for this experiment was spaced apart by $1/12\lambda$. For each curve (excluding the line $P_{FA} = 10^{-3}$), the results of 10^4 Monte-Carlo experiments were averaged to obtain the curves. The AMF tested every resolution cell on the angle-Doppler map. The probability of false alarm of a true CFAR detector should not change as a function of SINR of a target present somewhere in the search area. It is observed from the figure that the 12λ ULA AMF and the random array MP-CFAR detectors have probabilities of false alarm that are little changed as a function of the SNR of a target. More specifically, at low SNR the MP-CFAR experiences a probability of false alarm of about 2×10^{-3} instead of $P_{FA} = 10^{-3}$. This slight increase in the probability of false alarm occurs because at low SINR, the probability of correct recovery (the probability that MP-CFAR recovers the correct resolution cell to test) is less than one. As the SNR of the target increases, the probability of correct recovery increases, and the false alarm probability of MP-CFAR decreases to $P_{FA} = 10^{-3}$ as intended. It is also noticed that the AMF using a 12λ ULA experiences a slight increase in the probability of false alarm as the

SNR of the interfering target increases. In contrast, a random array using AMF cannot cope with energy leaked by high sidelobes, and as the strength of the target increases, the probability of false alarm increases.

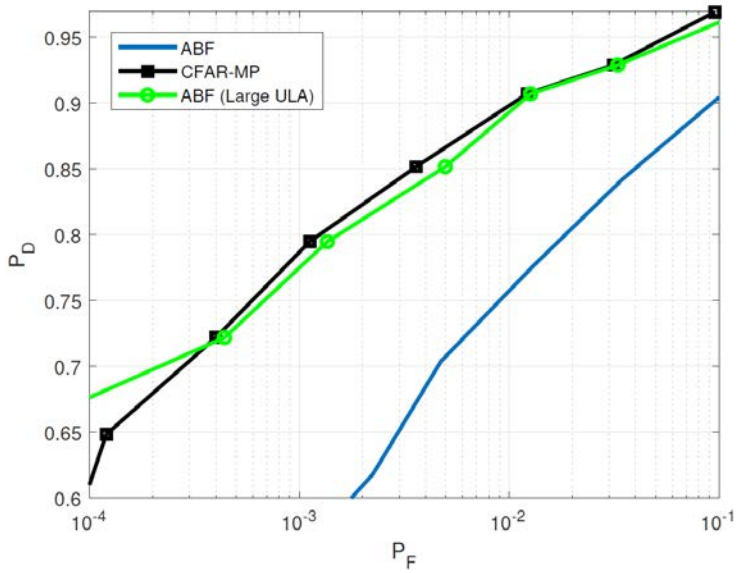

Figure 5: ROC curve for a single target for the AMF with a random array, MP-CFAR with a random array, and the AMF with a large ULA. Parameters SNR = 15.5 dB and CNR = 30 dB.

In Figure 5, are shown the receiver operating characteristic (ROC) curves of the AMF using a 12λ ULA, the AMF using a random array, and MP-CFAR using a random array, and for a single target in the field of view. The target again has the angle-Doppler pair (5/Z,0). From the figure, the large ULA using AMF performs well as expected. Since the ULA array does not exhibit large sidelobes, the target does not significantly increase the probability of false alarm. In contrast, it is seen that the AMF with the random array performs considerably worse. The random array has large sidelobes, and since the AMF does not account for the large sidelobes, the radar experiences a high false alarm rate. The MP-CFAR with a random array on the other hand performs similarly to the AMF with a large ULA. The MP-CFAR unlike the AMF, accounts for detected targets and removes the targets before detecting more targets. Note that the MP-CFAR performs similarly to the AMF with the large ULA using about 3/4s of the number of elements compared to the large ULA. This demonstrates the savings without loss of performance that are gained by random arrays and the proposed MP-CFAR detector.

6.0 CONCLUSIONS

In this paper we propose using a random array with the MP-CFAR algorithm to solve the target detection problem in a STAP setting. The random array is a large undersampled array that achieves high resolution due to the large aperture at the cost of high sidelobes. Although conventional beamforming cannot cope with the high sidelobes introduced by the random array, the proposed sparsity based algorithms can cope with the high

sidelobes allowing one to enjoy the high resolution of the random array without the consequences of the high sidelobes. This was achieved by the proposed algorithms by iteratively detecting targets one by one and removing their contributions from the data. Numerical simulations show that the proposed algorithms outperform beamforming methods when a random array is employed.

REFERENCES

[1] J. Ward, Space-time adaptive processing for airborne radar, DTIC Document, 1994.

[2] Y. Lo, "A mathematical theory of antenna arrays with randomly spaced elements," *IEEE Transactions on Antennas and Propagation*, vol. 12, no. 3, pp. 257-268, 1964.

[3] B. Stienberg, "The peak sidelobe of the phased array having randomly located elements," *IEEE Transactions on Antennas and Propagation*, vol. 20, no. 2, pp. 129-136, 1972.

[4] F. Athley, C. Engdahl and P. Sunnergren, "On radar detection and direction finding using sparse arrays," *IEEE Transactions on Aerospace and Electronic Systems*, vol. 43, no. 4, pp. 1319-1333, 2007.

[5] L. Carin, "On the Relationship Between Compressive Sensing and Random Sensor Arrays," *IEEE Antennas and Propagation Magazine*, vol. 51, no. 5, pp. 72-81, 2009.

[6] D. L. Donoho, "Compressed Sensing," *IEEE Transactions on information theory*, vol. 52, no. 4, pp. 1289-1306, 2006.

[7] J. A. Tropp and A. C. Gilbert, "Signal recovery from random measurements via orthogonal matching pursuit," *IEEE Transactions on information*, vol. 53, no. 12, pp. 4655-4666, 2007.

[8] W. Dai and O. Milenkovic, "Subspace pursuit for compressive sensing: Closing the gap between performance and complexity," DTIC Document, Tech. Rep., 2008.

[9] D. Needell and J. A. Tropp, "CoSaMP: Iterative signal recovery from incomplete and inaccurate samples," *Elsevier*, vol. 26, no. 3, pp. 301-321, 2009.

[10] M. Rossi and A. M. Haimovich, "Compressive sensing with unknown parameters," *2012 Conference Record of the Forty Sixth Asilomar Conference on Signals, Systems and Computers (ASILOMAR)*, pp. 436-440, 2012.

[11] M. E. Davies and Y. C. Eldar, "Rank awareness in joint sparse recovery," *IEEE Transactions on Information Theory*, vol. 58, no. 2, pp. 1135-1146, 2012.

[12] J. A. Tropp and S. J. Wright, "Computational methods for sparse solution of linear inverse problems," *Proceedings of the IEEE*, vol. 98, no. 6, pp. 948-958, 2010.

[13] M. Rossi, A. M. Haimovich and Y. C. Eldar, "Spatial compressive sensing in MIMO radar with random arrays," *Information Sciences and Systems (CISS), 2012 46th Annual Conference on*, pp. 1-6, 2012.

[14] J. Ward, "Space-time adaptive processing for airborne radar," *Space-Time Adaptive Processing (Ref. No. 1998/241), IEE Colloquium on*, pp. 2/1-2/6, 1988.

[15] J. Ward, " Space-time adaptive processing with sparse antenna arrays," *Signals, Systems and Computers, 1998. Conference Record of the Thirty-Second Asilomar Conference*, vol. 2, pp. 1537-1541, 1998.

[16] F. C. Robey, D. R. Fuhrmann, E. J. Kelly, and R. Nitzberg, "A CFAR adaptive matched filter detector," *IEEE Transactions on Aerospace and Electronic Systems*, vol. 28, no. 1, pp. 208-216, 1992.

[17] M. Elad, Sparse and Redundant Representations: From Theory to Applications in Signal and Image Processing, New York: Springer, 2010.

[18] J. Liu, H. Li, and B. Himed, "Threshold setting for adaptive matched filter and adaptive coherence estimator," *IEEE Signal Processing Letters*, vol. 22, no. 1, pp. 11-15, 2015.